ROYAL SOCIETY OF CHEMISTRY

COMMUNICATION

Check for updates

Frequency-dependent stimulated and post-stimulated voltage control of magnetism in transition metal nitrides: towards brain-inspired magneto-ionics†

Zhengwei Tan, [ID] [a] Julius de Rojas,[a] Sofia Martins, [ID] [a] Aitor Lopeandia,[ab] Alberto Quintana,[c] Matteo Cialone,[d] Javier Herrero-Martín,[e] Johan Meersschaut, [ID] [f] André Vantomme, [ID] [g] José L. Costa-Krämer, [ID] [h] Jordi Sort [ID] *[ai] and Enric Menéndez [ID] *[a]

Magneto-ionics, which deals with the change of magnetic properties through voltage-driven ion migration, is expected to be one of the emerging technologies to develop energy-efficient spintronics. While a precise modulation of magnetism is achieved when voltage is applied, much more uncontrolled is the spontaneous evolution of magneto-ionic systems upon removing the electric stimuli (*i.e.*, post-stimulated behavior). Here, we demonstrate a voltage-controllable N ion accumulation effect at the outer surface of CoN films adjacent to a liquid electrolyte, which allows for the control of magneto-ionic properties both during and after voltage pulse actuation (*i.e.*, stimulated and post-stimulated behavior, respectively). This effect, which takes place when the CoN film thickness is below 50 nm and the voltage pulse frequency is at least 100 Hz, is based on the trade-off between generation (voltage ON) and partial depletion (voltage OFF) of ferromagnetism in CoN by magneto-ionics. This novel effect may open opportunities for new neuromorphic computing functions, such as post-stimulated neural learning under deep sleep.

New concepts

We propose an approach to control the magnetization evolution of electrolyte-gated CoN-based heterostructures both during (stimulated) and after (post-stimulated) voltage actuation by means of electric-field-driven transport of N ions. Specifically, upon voltage removal (*i.e.*, once voltage stimuli are off), magnetization in our magneto-ionic systems can be either reduced or increased, without any further energy input, depending on the interplay between film thickness and the prior voltage actuation protocols. The latter offers a new logical function that enables, for instance, the possibility to mimic neuromorphic learning under deep sleep. Such functionality cannot be emulated with existing types of neuromorphic materials (*e.g.*, resistive switching or spintronic materials). Here, post-stimulated magneto-ionic control is possible by a voltage-driven N ion accumulation effect at the outer surface of CoN films adjacent to a liquid electrolyte, which is generated for sufficiently thin CoN films and high voltage actuation frequencies, thus offering a new concept, at the materials level, for advanced brain-inspired computing functions.

Introduction

Magneto-ionics, relying on the control of magnetic properties through voltage-driven ion (O^{2-},[1–5] H^+,[6–8] Li^+,[9] F^-[10] or N^{3-}[11–14]) migration, holds potential for being one of the technologies to develop low-power memory applications. In recent years, significant progress has been made in improving ion motion rates and endurance, which are the two main bottlenecks to exploit the full potential of magneto-ionics at room temperature. This has been achieved by proper selection of the moving ion species, target materials, heterostructure designs, electrolytes and voltage actuation protocols. These advances have made it possible to propose magneto-ionic materials as suitable candidates for new spintronic applications,[15,16] as well as for new computation paradigms, such as neuromorphic systems.[17,18] The precise modulation of magnetism by magneto-ionics has been already successful to emulate the main synaptic functions: activation threshold, plasticity (potentiation and depression),

[a] *Departament de Física, Universitat Autònoma de Barcelona, E-08193 Cerdanyola del Vallès, Spain. E-mail: jordi.sort@uab.cat, enric.menendez@uab.cat*

[b] *Catalan Institute of Nanoscience and Nanotechnology (ICN2), CSIC and BIST, Campus UAB, Cerdanyola del Vallès, E-08193 Barcelona, Spain*

[c] *Institut de Ciència de Materials de Barcelona (ICMAB-CSIC), Campus UAB, Bellaterra, E-08193 Barcelona, Spain*

[d] *CNR-SPIN Genova, Corso F. M. Perrone 24, 16152 Genova, Italy*

[e] *ALBA Synchrotron Light Source, 08290 Cerdanyola del Vallès, Spain*

[f] *IMEC, Kapeldreef 75, B-3001 Leuven, Belgium*

[g] *Quantum Solid State Physics, KU Leuven, Celestijnenlaan 200 D, B-3001 Leuven, Belgium*

[h] *IMN-Instituto de Micro y Nanotecnología (CNM-CSIC), Isaac Newton 8, PTM, 28760 Tres Cantos, Madrid, Spain*

[i] *Institució Catalana de Recerca i Estudis Avançats (ICREA), Pg. Lluís Companys 23, E-08010 Barcelona, Spain*

† Electronic supplementary information (ESI) available. See DOI: https://doi.org/10.1039/d2mh01087a

spike-magnitude dependence, spike-timing-dependent plasticity, spike-rate-dependent plasticity and forgetting.[17,18] Plasticity is linked to learning and memory, and, in particular, spike-rate-dependent plasticity is considered the most accurate model to describe learning and memory.[19–24]

Among materials to mimic synapses, magneto-ionic systems stand out from phase-change compounds,[25] resistive-switching oxides[20,26–28] or spintronic multilayers[21,23] basically due to the potential improvement of energy efficiency, envisaging ultra-low power hardware with minimized Joule heating effects.[29–31] In addition, magneto-ionics could exploit the extra degree of freedom provided by the vector nature of magnetization which may allow synapses to be directly programmed with positive and negative synaptic weights without need of additional electronics.[17] However, while the weight (e.g., resistance,[20,22,26,28] magnetization[21,23]) update in most current non-volatile technologies can be manipulated by changing the input electric signal (value and sign), the post-stimulated (without input) states are usually not controllable due to system-inherent relaxation effects.[32,33] This post-stimulus uncontrollability greatly limits the emulation of some important brain-inspired functions, such as maintaining learning efficiency even during deep sleep.[34] Therefore, procedures capable of controlling post-stimulated evolution while maintaining good tunability in modulation of weight update are highly desired.

Here, we propose a new approach to control the magnetization evolution both in stimulated and post-stimulated states based on voltage-driven ferromagnetism in CoN-based heterostructures through the transport of N^{3-} ions, with a cumulative 10^{-2} s ion motion response. By application of successive voltage pulses, information processing, memory (retention), recovering or self-evolution by maturity (i.e., controllable updating even when a voltage is no longer applied) can be emulated in a controlled manner. Such control is possible by tuning the CoN film thickness (which determines ion motion rates) and the pulse frequency. The observed effects result from the trade-off between generation (voltage ON) and partial depletion (voltage OFF) of magnetization. Besides boosting energy efficiency, this approach offers an important additional logical function: after voltage has been applied, the device can be either programmed to learn or forget without any further energy input, thus mimicking synaptic functions under deep sleep, when processing of information can continue without any external signal input.

Experimental

Sample preparation

CoN films with thicknesses ranging from 5 to 200 nm were grown using reactive sputtering, as described earlier.[11] A 20 nm Ti and 60 nm Cu buffer layers were first prepared by sputtering on B-doped, highly conducting [100]-oriented Si wafers (60 nm Cu/20 nm Ti/0.5 mm [100]-oriented Si). The CoN films were grown in a home-made triode sputtering system with a base pressure as low as 10^{-8} Torr to provide an ultra-high vacuum, oxygen-free growth condition, and exclude interferences of

oxygen magneto-ionics. Prior to CoN deposition, a portion of the Cu/Ti/Si substrate was masked to make the required electric contact on Cu for in situ magnetoelectric experiments. The distance between the target and the substrate was approximately 10 cm and the sputtering rate was about 1 Å s^{-1}. CoN was grown under a total pressure of 8×10^{-3} Torr with an atmosphere of N2 : Ar =1 : 1.

Magneto-ionic characterization

In-plane magnetization was measured at room temperature using a commercial vibrating sample magnetometer (VSM) from Micro Sense (LOT-Quantum Design), with a maximum applied magnetic field of 2 T. The CoN samples were electrolyte-gated (with an external Agilent B2902A power supply). A Pt wire was used as counter electrode, whereas the working electrode was the investigated CoN/Cu/Ti/Si film. (i.e., home-made electrochemical capacitor geometry). Negative voltages here mean that negative charges accumulate at the working electrode (and vice versa for positive voltages). Anhydrous propylene carbonate with Na$^+$ and OH$^-$ solvated species (5–25 ppm) was used as electrolyte. Metallic sodium was immersed in the electrolyte to react with any traces of water. The magnetization (M) arises from normalizing the magnetic signal to the sample volume mounted in the electrolyte. Note that the linear background of the hysteresis loops (stemming from paramagnetic and diamagnetic contributions) was removed using the signal at high fields (i.e., fields always far above saturation fields).

Structural and compositional measurements

$\theta/2\theta$ X-ray diffraction (XRD) patterns were measured on a Materials Research Diffractometer (MRD) from Malvern PANalytical company, equipped with a PIXcel^{1D} detector, using Cu Kα radiation. High-resolution transmission electron microscopy (HRTEM), high-angle annular dark-field scanning transmission electron microscopy (HAADF-STEM), and electron energy loss spectroscopy (EELS) were performed on a TECNAI F20 HRTEM/STEM microscope operated at 200 kV. Cross sectional lamellae were prepared by focused ion beam and placed onto a Cu transmission electron microscopy grid. X-ray absorption spectroscopy (XAS) at the Co L$_{2,3}$ edges was performed using the BL29-BOREAS beamline at ALBA Synchrotron Light Source (Barcelona, Spain).[35] The spectra were measured in total electron yield (TEY), under ultra-high vacuum conditions (10^{-7} Torr) and at room temperature (300 K). For the elastic recoil detection (ERD) analysis, an impinging ion beam of 9.6 MeV 79Br^{5+} particles was used. The sample was tilted to a grazing incidence angle of 20° between the ion beam and the surface of the film. The elastic collision between the impinging nuclei and target atoms can result in recoiling target species. The mass, energy and probability of the atoms emitted from the sample in forward direction were recorded by means of a multi-dispersive detector telescope.[36] ERD analysis yields a quantitative elemental depth profile of the sample, including that of light elements.

Results and discussion

Enhancing ion motion by film thickness reduction: enabling magneto-ionics for brain-inspired computing

To investigate magneto-ionics, CoN films with a thickness ranging from 5 to 200 nm were electrolyte-gated in an electrochemical capacitor configuration using a Pt wire as counter electrode (as sketched in Fig. 1a),[3,11] while performing in-plane vibrating sample magnetometry (VSM). As shown in Fig. 1b, an anhydrous polar liquid electrolyte (propylene carbonate, PC, with Na^+ and OH^- solvated species)[37,38] was employed to allow the formation of an electric double layer (EDL)[39] and to serve as a N ion reservoir.[11]

The as-grown CoN films are highly nanostructured (Fig. S1, ESI†) and textured along (111) (Fig. S2, ESI†). As seen in Fig. S3 (ESI†), the X-ray absorption spectra of 5 nm- and 25 nm-thick CoN films show virtually the same shape, suggesting that the CoN stoichiometry is generally preserved regardless of film thickness. As seen in Fig. S4 (ESI†), the as-grown films exhibit virtually no ferromagnetism ($M_S < 10$ emu cm^{-3}) in agreement with the paramagnetic character of polycrystalline CoN.[11] Consecutive hysteresis loops (each lasting 30 min) were recorded while electrolyte-gating to track the evolution of magnetic properties with time and, thus, characterize the magneto-ionic response. Irrespectively of the film's thickness, all pristine CoN films exhibit magneto-ionic effects after being subjected to a DC voltage of −25 V, confirming voltage-driven transport of N^{3-} ions (Fig. S4 and Table S1, ESI†).[11] As also seen in Fig. S4 (ESI†), the timescale to achieve a steady magnetic hysteresis

loop turns out to be highly dependent on the CoN film thickness. Since the largest generation of magnetization takes place during the first 5 min (*i.e.*, during the descending branch of the first hysteresis loop), saturation magnetization measurements as a function of time were recorded while electrolyte-gating at −25 V to properly determine the ion motion rates at the beginning of the magneto-ionic effect from saturation magnetization changes (Fig. 1c and d). For this, an external magnetic field of 10 kOe, above the anisotropy field of the generated ferromagnetic Co, was applied to ensure magnetic saturation. At the initial stages of voltage actuation, the rate of magnetization generation increases as the CoN film thickness decreases. This generation of magnetization reaches saturation (*i.e.*, showing a steady M_S) faster for thin than for thick films. However, the achieved steady value of M_S increases with film thickness (Table S1, ESI†) in agreement with the results of consecutive magnetic hysteresis loops recorded under the same voltage actuation (Fig. S4, ESI†). In addition, the steady coercivities H_C and squareness M_R/M_S (%) follow a dissimilar trend with thickness reduction. While coercivity decreases with film reduction, squareness increases, suggesting that the generated ferromagnetic Co grows more uniformly, enhancing exchange interactions among Co clusters which are in detriment of coercivity.[40] Fig. 1d shows the time evolution of growth rates of generated magnetization for all CoN films obtained by differentiating M_S with respect to time t: dM_S/dt. This allows determining initial ion motion rates. An around 7.4-fold enhancement of the highest ion motion rate is achieved by reducing the thickness from 200 nm to 5 nm, showing that of

Fig. 1 Role of CoN film thickness in ion motion. (a) Schematic representation of the voltage actuation on CoN films by electrolyte-gating. (b) Sketch of the electric double layer (EDL) formed at the surface of the CoN films while electrolyte-gating at $\Delta V < 0$. (c) Saturation magnetization (M_S) as a function of time t for all the investigated CoN films under electrolyte-gating at −25 V while applying an external in-plane magnetic field of 10 kOe. (d) Derivative of the M_S (t) dependences: dM_S/dt of the results in panel (c).

0.8 emu cm^{-3} s^{-1} and 5.9 emu cm^{-3} s^{-1}, respectively. The latter represents the largest ion motion speed achieved so far in the self-contained magneto-ionic approach (see Table S2, ESI†).[11–13] Considering that 1 s is the time resolution of the employed magnetometer, all CoN films clearly exhibit sub-1s magneto-ionic response since the generated magnetic moment at 1 s is always larger than the highest sensitivity of the VSM (125 nemu), a value which implies changes in magnetic moment above the resolution of the setup (Fig. S5 and Table S1, ESI†). In Table S1 (ESI†), the ΔM in 1 s increases greatly as the thickness decreases, indicating a considerable improvement of the trigger efficiency of the magneto-ionic motion because of thickness reduction. This suggests feasibility of our approach as a framework for synaptic-like materials since synapse functions require responses to repeated 10^{-2} s stimuli.[41] The leap in ion motion for thinner films is mainly associated with the enhancement of the applied electric field due to film thickness reduction. In a first approximation, the system can be considered as a condenser-like structure with parallel plates (*i.e.*, parallel plate capacitor), as shown in Fig. 1b. Given a certain potential V, the electric field E is inversely proportional to active dielectric thickness (the total thickness of the CoN film plus the EDL).[42] Hence, the thinner the film, the thinner the active dielectric thickness and the more intense the electric field, providing a higher driving force to overcome the energy barrier for ion diffusion and to accelerate transport of nitrogen ions.

Dynamic (pulsed DC actuation) characterization of the magneto-ionic response: tuning the learning performance and emulation of 'self-learning by maturity' function (with no external voltage input)

Since communication among neurons is frequency-encoded, a dynamic characterization of the magneto-ionic response is crucial to determine its capability to mimic synaptic functions. Therefore, for magneto-ionic characterization, electrolyte-gating *via* electric voltage pulses was performed. Static constant voltages (DC) were used as reference. Fig. 2a shows schematically the voltage protocol used for the dynamic characterization: voltages square waves (from 0 V to −25 V) of period T (and corresponding frequency of $f = 1/T$) and pulse duration of $T/2$ (resulting in a duty cycle of 50%). The period was varied from 10^2 s to 10^{-2} s to obtain actuation frequencies from 10^{-2} Hz to 10^2 Hz. CoN films with thicknesses of 25 nm and 200 nm were chosen as representative heterostructures to characterize the magneto-ionic response during pulsed DC voltage actuation, due to their significantly different ion motion speed. Both films were electrolyte-gated at different frequencies for gating times of around 550 s and 900 s, respectively, to ensure reaching a saturated magnetization state. While gating, time-dependent magnetization measurements under an applied magnetic field of 10 kOe were recorded by VSM.

As can be seen in Fig. 2b, which corresponds to the magneto-ionic response of the 200 nm film, M_S gradually increases up to 248 emu cm^{-3} upon treatment at −25 V DC voltage for 900 s. Then, after turning off the voltage, M_S slightly

decays, in agreement with the partial magnetization depletion (*i.e.*, recovery) that occurs in these systems, which shares resemblance with a nitriding process of metallic Co.[11] From a synaptic-like viewpoint and taking saturation magnetization as synaptic weight, this allows mimicking plasticity (*i.e.*, change in magnetization with time). Specifically, potentiation (*i.e.*, magnetization increase, voltage on), representing learning, and depression (*i.e.*, magnetization reduction, voltage off), reproducing forgetting[17] can be mimicked. Fig. 2b also shows the evolution of M_S *vs. t* upon subjecting the 200 nm CoN films to voltage pulses of different frequency where the generated magnetization scales with frequency. As f increases from 1 to 100 Hz, the M_S values at 960 s increase one order of magnitude, from 17.6 to 168.2 emu cm^{-3} (see also Fig. S6, ESI†). Moreover, the steady M_S values and its recovery are also frequency dependent, emulating spike-rate-dependent plasticity. Resembling human brain, repeated spiking (*i.e.*, high frequency voltage pulsing) reinforces retention of information and thus learning.[43,44] Human learning also takes place by transforming 'short-term memory' (STM) into 'long-term memory' (LTM) through the increase in frequency of the voltage stimuli.[28] STM refers to the temporal storage of input information in the hippocampus, which lasts only a few seconds. By increasing the frequency of training and stimulation, information obtained from outside can be continuously transferred to and stored in the cerebral cortex for hours or even years (LTM). As depicted in Fig. 2b, this transition can be mimicked by voltage-driven generation of ferromagnetism in CoN through voltage pulse waves of different frequency. This learning emulation capacity raises from the pulsed DC actuation which results in a trade-off between generation (voltage ON) and partial depletion/recovery (voltage OFF) of magnetization. With increased frequency, generation of magnetization prevails over dynamic recovery, resulting in larger M_S values. As seen in Fig. S1b (ESI†), nitrogen migration when applying pulsed DC voltage actuation takes place *via* planar-migration fronts, similarly to CoN films subjected to DC voltage actuation,[11] suggesting that the ion motion mechanisms are independent from voltage actuation characteristics.

Conversely, the 25 nm-thick CoN films offer a completely different scenario, where trade-off between generation (voltage ON) and partial depletion (voltage OFF) of magnetization is strongly altered. Specifically, for DC and pulsed actuation at high frequencies (*i.e.*, 1, 10 and 100 Hz), once the voltage actuation is switched off (*i.e.*, after t = 620 s in Fig. 2c), the saturation magnetization increases (Fig. 2c), rather than decreasing (as for the 200 nm-thick film), hence emulating a self-learning process with no external stimulus. This suggests that, once voltage is switched off, an additional driving force is set in place in the thinner films to pump ions towards the electrolyte, which screens and, in fact, overcomes recovery. This self-learning effect is particularly obvious after non-pulsed DC voltage actuation (blue curve in Fig. 2c). Given the high motion rates of N^{3-} ions across the 25 nm-thick CoN films (much larger than for thicker films –see Table S1, ESI†) and the limited N^{3-} solubility in the liquid electrolyte,[45,46] a N^{3-} ion accumulation
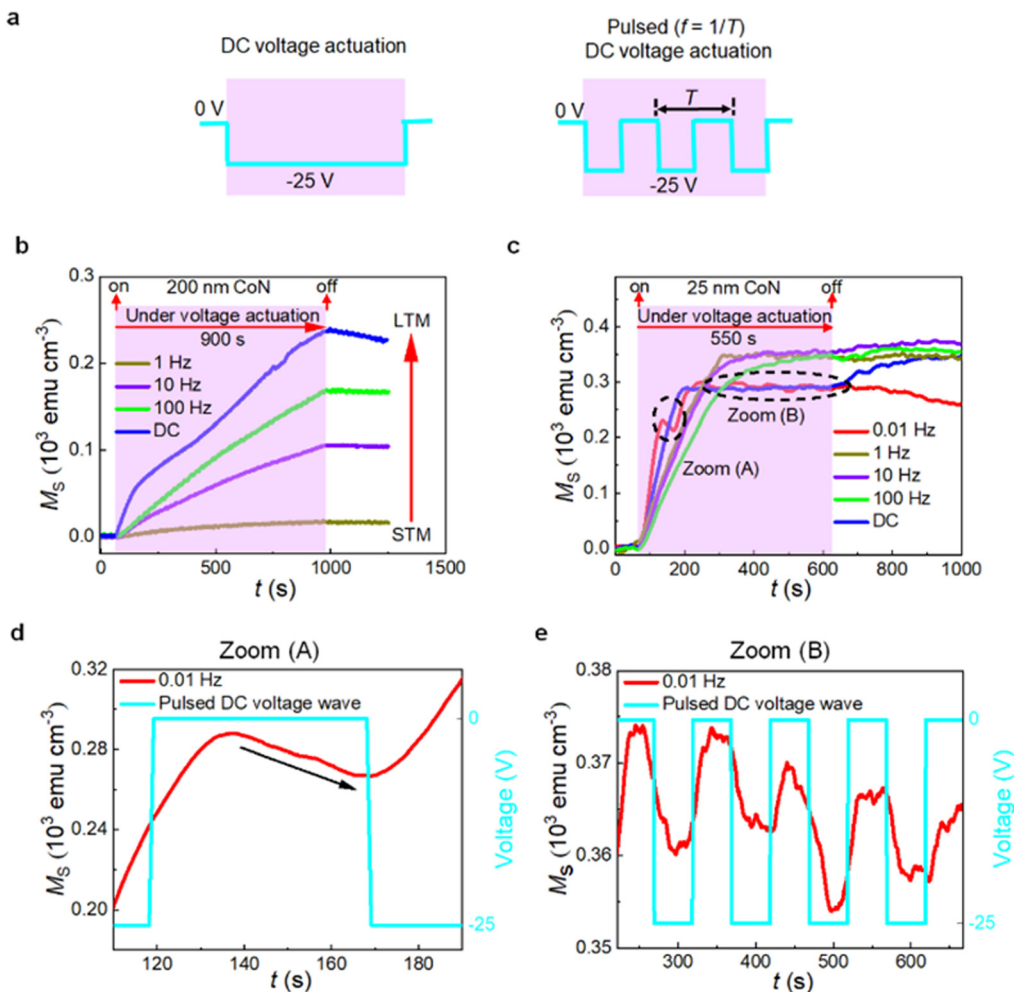
Fig. 2 Pulsed DC (dynamic) voltage actuation. (a) Schematic representation of the DC and pulsed DC voltage actuations. (b) Time evolution of the saturation magnetization (M_S *vs. t*) while electrolyte-gating at −25 V with DC and pulsed DC (at *f* from 1 to 100 Hz) voltages for the 200 nm CoN film. STM and LTM represent the short-term memory and the long-term memory, respectively. (c) Time evolution of the saturation magnetization (M_S *vs. t*) while electrolyte-gating at −25 V with DC and pulsed DC voltages (at *f* from 0.01 Hz to 100 Hz) for the 25 nm CoN film. (d) Zoom (A) of panel (c). (e) Zoom (B) of panel (c).

effect at the interface between the magneto-ionic film and the liquid reservoir is envisaged. Due to the N^{3-} concentration gradient, these ions will be presumably released to the electrolyte once voltage is switched off (following Fick's laws[47]), leading to the increase of M_S. Note that whereas the frequency influence on M is clear, the larger M at higher frequency may also be due to the larger number of applied pulses, which results in more nitrogen ion movement and, thus, higher amounts of Co formed behind.

Remarkably, compared with 25 nm-thick CoN films, the 50 nm-thick ones display a weaker increase of M_S when the voltage actuation is turned off (Fig. S7, ESI†) whereas the 200 nm-thick films do not show this effect at all (Fig. 2b), indicating that the voltage-driven ion motion rate across the film is sufficiently slow in that case. Thus, the ion motion rate is a critical parameter to observe ion accumulation. As seen in Fig. S7 (ESI†), this voltage-free magnetization generation is limited in time since, after a while, magnetization recovery

starts (after 170 s for 50 nm and after 695 s for 25 nm thick films). This effect becomes less pronounced when the actuation frequency is decreased. In such a case, dynamic recovery occurs already during the $\Delta V = 0$ V intervals of the pulse voltage actuation, precluding the ion accumulation effect at the interface between the CoN films and the electrolyte (Fig. 2c). Indeed, when using a frequency of 0.01 Hz, recovery can be clearly observed upon voltage actuation (Fig. 2c and d), during the subsegments with $\Delta V = 0$ V. Fig. 2d and e show two zooms of the M_S *vs. t* dependencies for voltage actuations at a frequency of 0.01 Hz. In zoom (A), a rise followed by a continuous depletion of M_S can be clearly seen (Fig. 2d). Zoom (B) indicates that the system exhibits an effective cyclability due to the trade-off between generation and magnetization recovery (Fig. 2e). Partial cyclability can be reproduced without the need of biases of opposite polarity, providing an energy-efficient and endurable way to cycle the system, since repeatedly switching voltage polarities is often linked to degradation. Remarkably, this ion

accumulation effect can be tuned by controlling just two external parameters: the CoN film thickness, which largely determines the ion motion speed, and the frequency of the pulsed voltage actuation. This demonstrates that it is possible to tune learning and forgetting at will by solely modifying the voltage actuation frequency since this parameter allows tuning the interplay between magnetization generation, recovery and, thus, ion accumulation at the CoN film/reservoir interface. Existing emulation of learning in artificial intelligence heavily relies on external inputs, which makes it difficult to simulate some synaptic functions under deep sleep, when information retention can continue even after stopping the input signal. In fact, the possibility of learning even without stimulus is analogous to a 'learning by maturity' process, *i.e.*, the possibility to remember fine details after resting. During sleep, biological synapses relax but maintain the brain's neuroplasticity and the ability to learn.[34] Recently, incorporation of slow-wave sleep periods has been shown advantageous also for artificial neuromorphic computing algorithms, to enhance the dynamical computation stability.[48] Remarkably, the reported effect could also be understood as a useful method to simulate overstimulation and neuronal malfunction.[49]

Microscopic mechanism behind the magneto-ionic emulation of the self-learning neuromorphic function Fig. 3a schematically shows the M_S *vs. t* evolution for systems displaying and lacking the ion accumulation effect, respectively. If we define M_{S0} as the steady saturation magnetization achieved while actuating with voltage and M_{S1} the saturation magnetization reached within a short period of time after removing the voltage, the sign of the difference between M_{S0} and M_{S1} will represent the existence or absence of the ion accumulation effect: $M_{S0}–M_{S0} > 0$ (no accumulation) and $M_{S0}–M_{S0} < 0$ (accumulation). The ion accumulation effect at the surface of the CoN layer can be understood as the interplay between several dynamic processes at the atomic level. Highlighted among them are: (1) conventional electric-field-induced N^{3-} ion migration across CoN towards the electrolyte[11] (represented by a velocity v_E), (2) redistribution (*i.e.*, intermixing) between solvated N^{3-} ions (identified as N-PC) and N-free PC molecules driven by the gradient[50–52] in number of PC molecules carrying N^{3-} along the direction perpendicular to the interface (the velocity of this redistribution process is represented by v_{Red}), (3) diffusion of N^{3-} ions accumulated at the interface (v_A), and (4) N^{3-} ion recovery from the electrolyte to the CoN film (v_{Rec}).[11] Fig. 3b schematically depicts the generation of magnetization in a thin CoN from an atomistic viewpoint that shows ion accumulation effects. When a negative voltage is applied, N^{3-} ions continuously migrate towards the electrolyte, leaving behind Co-rich areas in the CoN film responsible for the increase in saturation magnetization (stage (i) in Fig. 3b). Concomitantly, N^{3-} dissolution takes above. However, after a while, the generation of saturation magnetization slows down, tending to saturate (stage (ii) in Fig. 3b). This is ascribed to the fact that the N^{3-} ion migration occurs faster than the redistribution of PC molecules, thus limiting further dissolution of N^{3-}ions into the electrolyte (due to the limited N solubility in
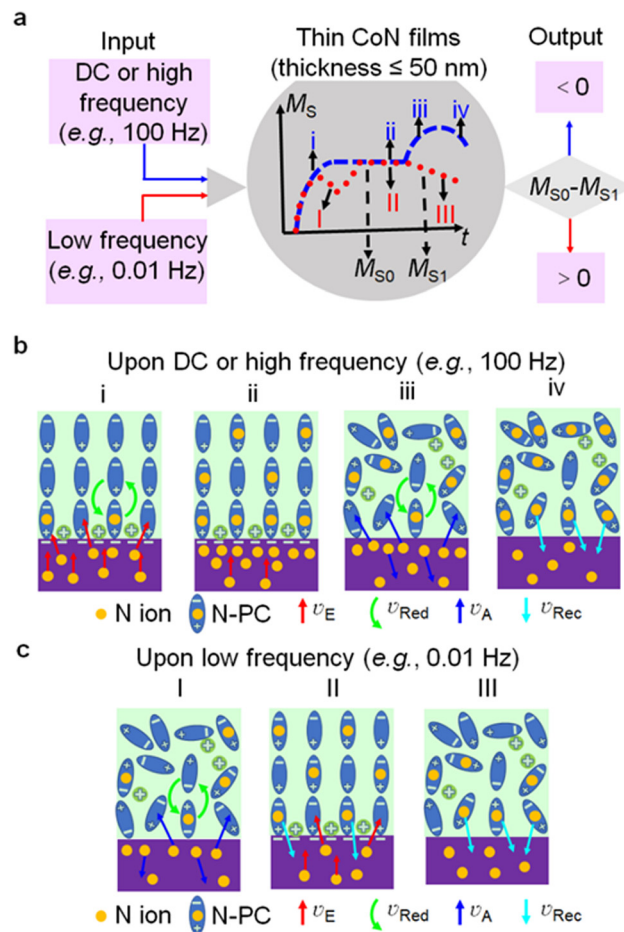

Fig. 3 Frequency dependence of the ion accumulation effect. (a) Schematic representation of the typical M_S *vs. t* dependences of heterostructures with thin CoN films (thicknesses ≤ 50 nm) showing (DC and pulsed DC at a frequency ≥ 1 Hz: blue dashed line) or not showing (pulsed DC at a frequency < 1 Hz: red dots) an ion accumulation interfacial effect. (b) (c) microscopic mechanisms for the existence and absence of ion accumulation, respectively. v_E, v_{Red}, v_A, v_{Rec} represent the speed of N ion migration in CoN, redistribution of PC molecules, migration of accumulated N ions, and N ion recovery, respectively. For simplicity, N denotes N^{3-} in the picture.

PC, *i.e.*, absence of N-free PC molecules) and forcing N^{3-} ions to accumulate at the surface of the CoN film. After switching the voltage off, the concentration gradient between PC molecules tends to balance, further redistributing regular PC molecules and PC molecules saturated with N^{3-}. In this way, some regular PC molecules are able to reach the interface, providing more sites to incorporate N and, thus, to dissolve it. At the same time, the accumulated N^{3-} ions at the upper part of the CoN films can diffuse into the electrolyte and inside the CoN films (*i.e.*, towards the inner parts of the film, which normally occurs quite slowly). The former process, *i.e.*, N dissolving in the electrolyte, is the mechanism behind the increase in M_S even without voltage (stage (iii) in Fig. 3b). After some time, the N^{3-} diffusion process in the film weakens due to the decreasing concentration gradient and becomes surpassed by the conventional ion recovery process, which accounts for the decrease in M_S (stage (iv) in Fig. 3b). Remarkably, ion accumulation takes
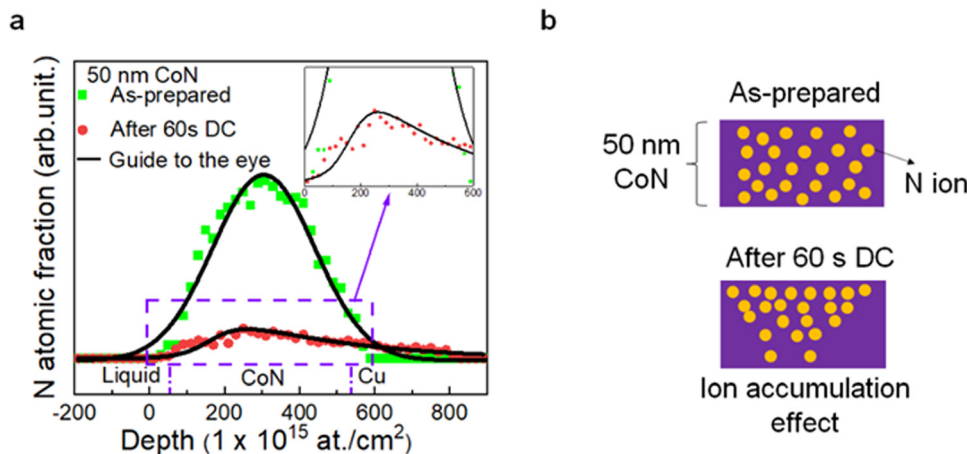
Fig. 4 Direct proof of the ion accumulation effect. (a) Elastic recoil detection measurements revealing the N depth distribution of an as-prepared and an actuated (−25 V DC voltage for 60 s) 50 nm-thick film, with a zoomed-in view of the area surrounded by the purple dashed box. (b) Cartoon representing the N ion distribution in an as-prepared sample and an actuated sample showing the ion accumulation effect.

place only in thin films (thickness $\leq$ 50 nm), since they exhibit sufficiently high voltage-driven ion motion (*i.e.*, v_E) values when actuated with either DC or pulsed DC voltage at high frequencies ($f \geq$ 1, 10 and 100 Hz). Fig. 3c shows the atomistic mechanism when the heterostructure does not show ion accumulation effects, which corresponds to the situation in which the frequency of the pulsed DC actuation is low (*e.g.*, f = 0.01 Hz). Even though weak ion accumulation effects are feasible (stage (I)), they tend to rapidly vanish due to the long voltage interruption between the consecutive pulses, facilitating recovery processes and thus causing a partial magnetization depletion (stages (II) and (III)) during pulsing, as experimentally seen in Fig. 2c and e and depicted in the red dotted curve of Fig. 3a.

With the goal of obtaining direct evidence of this ion accumulation effect at the interface between the film and the electrolyte, the N^{3-} depth distribution of a 50 nm-thick sample upon DC voltage actuation has been assessed by elastic recoil detection analysis. As clearly seen in Fig. 4a, the depth distribution of N^{3-} for as-prepared CoN films is symmetric but becomes asymmetric during the DC voltage treatment. After applying a short 60 s DC voltage, this distribution is positively skewed, confirming that the N^{3-} content at the upper part of the film is larger than that at the bottom (*i.e.*, deeper) region and, thus, validating the ion accumulation effect (Fig. 4b).

Conclusion

Our work demonstrates a controllable ion accumulation effect at the interface between the CoN films and the adjacent electrolyte, which is set by a proper selection of the CoN film thickness and the pulse frequency of the voltage actuation. This effect, which takes place when the CoN film thickness is below 50 nm and the voltage pulse frequency is at least 100 Hz, is based on the trade-off between generation (voltage ON) and partial depletion (voltage OFF) of ferromagnetism in CoN by magneto-ionics. This effect allows for both the control of

magneto-ionic properties both while and upon removing voltage pulse actuation (effect off and on, resulting in stimulated and post-stimulated behaviour, respectively), expanding the potential of magneto-ionics in the emulation of post-stimulated neuromorphic functions, such as neural learning under deep sleep.

Author contributions

Z. T., J. S. and E. M. designed the experiment and the study. J. L. C.-K. synthesized the material. Z. T., S. M., A. Q., J. S. and E. M. carried out the VSM measurements and analysed the data. Z. T. and J. L. C.-K. performed the XRD characterization. Z. T. and A. L. prepared the cross-section lamellae for TEM. Z. T., A. L., J. S. and E. M. performed the HRTEM, STEM-HAADF and EELS and the corresponding data analysis. Z. T., J. deR., M. C. and J. H.-M. conducted the XAS experiments. J. M. and A. V. carried out the elastic recoil detection (ERD) analysis. All authors discussed the results and commented on the article. The article was written by Z. T., J. S. and E. M.

Conflicts of interest

There are no conflicts to declare.

Acknowledgements

References

1 U. Bauer, L. Yao, A. J. Tan, P. Agrawal, S. Emori, H. L. Tuller, S. van Dijken and G. S. D. Beach, *Nat. Mater.*, 2015, **14**, 174.

2 D. A. Gilbert, A. J. Grutter, E. Arenholz, K. Liu, B. J. Kirby, J. A. Borchers and B. B. Maranville, *Nat. Commun.*, 2016, **7**, 12264.

3 J. de Rojas, A. Quintana, A. Lopeandía, J. Salguero, J. L. Costa-Krämer, L. Abad, M. O. Liedke, M. Butterling, A. Wagner, L. Henderick, J. Dendooven, C. Detavernier, J. Sort and E. Menéndez, *Adv. Funct. Mater.*, 2020, **30**, 2003704.

4 A. Quintana, E. Menéndez, M. O. Liedke, M. Butterling, A. Wagner, V. Sireus, P. Torruella, S. Estradé, F. Peiró, J. Dendooven, C. Detavernier, P. D. Murray, D. A. Gilbert, K. Liu, E. Pellicer, J. Nogues and J. Sort, *ACS Nano*, 2018, **12**, 10291.

5 M. Cialone, A. Nicolenco, S. Robbennolt, E. Menéndez, G. Rius and J. Sort, *Adv. Mater. Interfaces*, 2021, **8**, 2001143.

6 A. J. Tan, M. Huang, C. O. Avci, F. Büttner, M. Mann, W. Hu, C. Mazzoli, S. Wilkins, H. L. Tuller and G. S. D. Beach, *Nat. Mater.*, 2019, **18**, 35.

7 M. Gößler, M. Albu, G. Klinser, E. M. Steyskal, H. Krenn and R. Würschum, *Small*, 2019, **15**, 1904523.

8 X. Ye, H. K. Singh, H. Zhang, H. Geßwein, M. R. Chellali, R. Witte, A. Molinari, K. Skokov, O. Gutfleisch, H. Hahn and R. Kruk, *Nat. Commun.*, 2020, **11**, 4849.

9 S. Dasgupta, B. Das, M. Knapp, R. A. Brand, H. Ehrenberg, R. Kruk and H. Hahn, *Adv. Mater.*, 2014, **26**, 4639.

10 S. Vasala, A. Jakob, K. Wissel, A. I. Waidha, L. Alff and O. Clemens, *Adv. Electron. Mater.*, 2020, **6**, 1900974.

11 J. de Rojas, A. Quintana, A. Lopeandía, J. Salguero, B. Muñiz, F. Ibrahim, M. Chshiev, A. Nicolenco, M. O. Liedke, M. Butterling, A. Wagner, V. Sireus, L. Abad, C. J. Jensen, K. Liu, J. Nogués, J. L. Costa-Krämer, E. Menéndez and J. Sort, *Nat. Commun.*, 2020, **11**, 5871.

12 J. de Rojas, J. Salguero, F. Ibrahim, M. Chshiev, A. Quintana, A. Lopeandia, M. O. Liedke, M. Butterling, E. Hirschmann, A. Wagner, L. Abad, J. L. Costa-Krämer, E. Menéndez and J. Sort, *ACS Appl. Mater. Interfaces*, 2021, **13**, 30826.

13 J. de Rojas, J. Salguero, A. Quintana, A. Lopeandia, M. O. Liedke, M. Butterling, A. G. Attallah, E. Hirschman, A. Wagner, L. Abad, J. L. Costa-Krämer, J. Sort and E. Menéndez, *Phys. Rev. Appl.*, 2021, **16**, 034042.

14 Z. Tan, S. Martins, M. Escobar, J. De Rojas, F. Ibrahim, M. Chshiev, A. Quintana, A. Lopeandia, J. L. Costa-Krämer, E. Menéndez and J. Sort, *ACS Appl. Mater. Interfaces*, 2022, **14**, 44581.

15 L. Herrera Diez, R. Kruk, K. Leistner and J. Sort, *APL Mater.*, 2021, **9**, 050401.

16 Y. Gu, C. Song, Q. Wang, W. Hu, W. Liu, F. Pan and Z. Zhang, *APL Mater.*, 2021, **9**, 040904.

17 R. Mishra, D. Kumar and H. Yang, *Phys. Rev. Appl.*, 2019, **11**, 054065.

18 S. Martins, J. De Rojas, Z. Tan, M. Cialone, A. Lopeandia, J. Herrero-Martín, J. L. Costa-Krämer, E. Menéndez and J. Sort, *Nanoscale*, 2022, **14**, 842.

19 J. Xiong, R. Yang, J. Shaibo, H.-M. Huang, H.-K. He, W. Zhou, X. Guo, J. Xiong, R. Yang, J. Shaibo, H. Huang, H. He, W. Zhou and X. Guo, *Adv. Funct. Mater.*, 2019, **29**, 1807316.

20 Z. Wang, S. Joshi, S. E. Savel'ev, H. Jiang, R. Midya, P. Lin, M. Hu, N. Ge, J. P. Strachan, Z. Li, Q. Wu, M. Barnell, G. L. Li, H. L. Xin, R. S. Williams, Q. Xia and J. J. Yang, *Nat. Mater.*, 2017, **16**, 101.

21 J. Torrejon, M. Riou, F. A. Araujo, S. Tsunegi, G. Khalsa, D. Querlioz, P. Bortolotti, V. Cros, K. Yakushiji, A. Fukushima, H. Kubota, S. Yuasa, M. D. Stiles and J. Grollier, *Nature*, 2017, **547**, 428.

22 H. Yeon, P. Lin, C. Choi, S. H. Tan, Y. Park, D. Lee, J. Lee, F. Xu, B. Gao, H. Wu, H. Qian, Y. Nie, S. Kim and J. Kim, *Nat. Nanotechnol.*, 2020, **15**, 574.

23 J. Grollier, D. Querlioz, K. Y. Camsari, K. Everschor-Sitte, S. Fukami and M. D. Stiles, *Nat. Electron.*, 2020, **3**, 360.

24 T. Ohno, T. Hasegawa, T. Tsuruoka, K. Terabe, J. K. Gimzewski and M. Aono, *Nat. Mater.*, 2011, **10**, 591.

25 W. Zhang, R. Mazzarello, M. Wuttig and E. Ma, *Nat. Rev. Mater.*, 2019, **4**, 150.

26 F. Zhou, Z. Zhou, J. Chen, T. H. Choy, J. Wang, N. Zhang, Z. Lin, S. Yu, J. Kang, H.-S. P. Wong and Y. Chai, *Nat. Nanotechnol.*, 2019, **14**, 776.

27 M. Prezioso, F. Merrikh-Bayat, B. D. Hoskins, G. C. Adam, K. K. Likharev and D. B. Strukov, *Nature*, 2015, **521**, 61.

28 J. Rao, Z. Fan, L. Hong, S. Cheng, Q. Huang, J. Zhao, X. Xiang, E.-J. Guo, H. Guo, Z. Hou, Y. Chen, X. Lu, G. Zhou, X. Gao and J.-M. Liu, *Mater. Today Phys.*, 2021, **18**, 100392.

29 M. Bibes and A. Barthélémy, *Nat. Mater.*, 2008, **7**, 425.

30 A. Molinari, H. Hahn and R. Kruk, *Adv. Mater.*, 2019, **31**, 1806662.

31 M. Nichterwitz, S. Honnali, M. Kutuzau, S. Guo, J. Zehner, K. Nielsch and K. Leistner, *APL Mater.*, 2021, **9**, 30903.

32 J. J. Yang and Q. Xia, *Nat. Mater.*, 2017, **16**, 396.

33 J. Tian, Z. Tan, Z. Fan, D. Zheng, Y. Wang, Z. Chen, F. Sun, D. Chen, M. Qin, M. Zeng, X. Lu, X. Gao and J.-M. Liu, *Phys. Rev. Appl.*, 2019, **11**, 024058.

34 S. Fattinger, T. T. de Beukelaar, K. L. Ruddy, C. Volk, N. C. Heyse, J. A. Herbst, R. H. R. Hahnloser, N. Wenderoth and R. Huber, *Nat. Commun.*, 2017, **8**, 15405.

35 A. Barla, J. Nicolás, D. Cocco, S. M. Valvidares, J. Herrero-Martín, P. Gargiani, J. Moldes, C. Ruget, E. Pellegrin and S. Ferrer, *J. Synchrotron Radiat.*, 2016, **23**, 1507.

36 J. Meersschaut and W. Vandervorst, *Nucl. Instrum. Methods Phys. Res., Sect. B*, 2017, **406**, 25.

37 C. Navarro-Senent, A. Quintana, E. Menéndez, E. Pellicer and J. Sort, *APL Mater.*, 2019, **7**, 030701.

38 G. G. Eshetu, G. A. Elia, M. Armand, M. Forsyth, S. Komaba, T. Rojo and S. Passerini, *Adv. Energy Mater.*, 2020, **10**, 2000093.

39 M. Weisheit, S. Fähler, A. Marty, Y. Souche, C. Poinsignon and D. Givord, *Science*, 2007, **315**, 349.

40 E. Menéndez, J. Demeter, J. van Eyken, P. Nawrocki, E. Jedryka, M. Wójcik, J. F. Lopez-Barbera, J. Nogués, A. Vantomme and K. Temst, *ACS Appl. Mater. Interfaces*, 2013, **5**, 4320.

41 C. C. McIntyre and R. W. Anderson, *J. Neurochem.*, 2016, **139**, 338.

42 D. Halley, N. Najjari, H. Majjad, L. Joly, P. Ohresser, F. Scheurer, C. Ulhaq-Bouillet, S. Berciaud, B. Doudin and Y. Henry, *Nat. Commun.*, 2014, **5**, 3167.

43 D. Hassabis, D. Kumaran, C. Summerfield and M. Botvinick, *Neuron*, 2017, **95**, 245.

44 D. Marković, A. Mizrahi, D. Querlioz and J. Grollier, *Nat. Rev. Phys.*, 2020, **2**, 499.

45 J. Read, K. Mutolo, M. Ervin, W. Behl, J. Wolfenstine, A. Driedger and D. Foster, *J. Electrochem. Soc.*, 2003, **150**, A1351.

46 W. Chen, M. Chen, M. Yang, E. Zou, H. Li, C. Jia, C. Sun, Q. Ma, G. Chen and H. Qin, *Appl. Energy*, 2019, **240**, 265.

47 I. M. Sokolov, J. Klafter and A. Blumen, *Phys. Today*, 2002, **55**, 48.

48 Y. Watkins, E. Kim, A. Sornborger and G. T. Kenyon. In Proceedings of the IEEE/CVF Conference on Computer Vision and Pattern Recognition Workshops, TN, USA, July, 2020.

49 H. Huang, C. Ge, Z. Liu, H. Zhong, E. Guo, M. He, C. Wang, G. Yang and K. Jin, *J. Semicond.*, 2021, **42**, 103103.

50 W. Guo, L. Cao, J. Xia, F.-Q. Nie, W. Ma, J. Xue, Y. Song, D. Zhu, Y. Wang and L. Jiang, *Adv. Funct. Mater.*, 2010, **20**, 1339.

51 A. Ozcan, C. Perego, M. Salvalaglio, M. Parrinello and O. Yazaydin, *Chem. Sci.*, 2017, **8**, 3858.

52 A. P. Thompson, D. M. Ford and G. S. Heffelfinger, *J. Chem. Phys.*, 1998, **109**, 6406.